Supplementary information

Tables and figures

Table S1: Characteristics of ASPC5-4 extracted from our previous publication [1]

[1] A.M. Ruban, G. Singh, R. Bahadur, C.I. Sathish, A. Vinu, Almond skin derived porous biocarbon nanoarchitectonics with tunable micro and mesoporosity for CO_2 adsorption and supercapacitors, Carbon 228 (2024) 119372.

ASPC5-4	
Surface area ($m^2\ g^{-1}$)	3535
Pore volume ($cm^3\ g^{-1}$)	1.96
Structure	Amorphous
Carbon (wt. %)	92.4
Hydrogen (wt. %)	0.48
Nitrogen (wt. %)	0.21
$Oxygen_{est}$ (wt. %)	6.9

est-estimated

Table S2: Quantification data for Fe and S from SEM and TEM EDS

Material	**TEM-EDS**		**SEM-EDS**	
	Fe (wt%/at%)	**S (wt%/at%)**	**Fe (wt%/at%)**	**S (wt%/at%)**
FeS-PC-1	-	-	0.80/0.18	0.87/0.34
FeS-PC-2	3.11/0.70	2.46/0.97	1.66/0.46	19.37/9.33
FeS-PC-3	-	-	0.37/0.12	35.95/20.30

Table S3: The crystallinity parameters extracted from powder X-ray diffraction (PXRD) data

Peak position 2θ (°)	**FWHM**	**D_p (nm)**	**Average D_p (nm)**
FeS-PC-1			
29.7801	1.3225	6.49	11.79
33.7996	0.6612	13.12	
43.7796	0.6612	13.52	
53.044	0.6612	14.02	
FeS-PC-2			
29.8585	0.3306	25.97	20.95
33.836	0.3306	26.23	
43.8233	0.6061	14.76	
53.1508	0.551	16.84	
FeS-PC-3			
29.8427	0.6612	12.99	13.41
33.7716	0.6612	13.11	
43.7484	0.6612	13.52	
53.0181	0.6612	14.02	

Note: For crystallite size measurement, the Scherrer's equation $D_p = K\lambda/(B\cos\theta)$ was used, wherein Dp is the crystallite size, K is Scherrer constant, λ is X-ray wavelength, B = Full width at half maximum (FWHM), and one half of the 2θ peak position.

Table S4: Full cell performance comparison of the FeS-PC-2 with the existing literature

Anode material	Cathode material	Specific capacity (mAh g^{-1})	Current density (A g^{-1})	Reference
C-felt	$LiFePO_4$ (LFP)	89 at 100th cycle	0.04	[1]
PHC@Si@SC	$LiNi_{0.8}Co_{0.1}Mn_{0.1}O_2$ (NCM811)	133 at 1st cycle	0.1	[2]
RP@P-PC	$LiFePO_4$ (LFP)	164 at 1st cycle	0.5	[3]
PCNSs	$LiNi_{1/3}Co_{1/3}Mn_{1/3}O_2$ (NCM111)	167 at 500th cycle	0.2	[4]
FeS-PC-2	**$LiCoO_2$ (LCO)**	**102 at 3rd cycle**	**0.1**	**This work**

Notes: C-felt - mesh-like carbon cloth, Si/Cu/void@C-14 - porous structure silicon/carbon composite, PHC@Si@SC - hierarchical porous hard carbon@Si@soft carbon material, RP@P-PC – Phosphorus-doped porous carbon, PCNSs – Porous carbon nanosheets derived from sodium humate

[1] V. Watson, Y.D. Yeboah, M.H. Weatherspoon, E.E. Kalu, Free-Standing and Binder-Free Porous Carbon Cloth (C-Felt) Anodes for Lithium-Ion Full Batteries, Batteries 11(3) (2025) 111.

[2] D. Lv, L. Yang, R. Song, H. Yuan, J. Luan, J. Liu, W. Hu, C. Zhong, A hierarchical porous hard carbon@Si@soft carbon material for advanced lithium-ion batteries, Journal of Colloid and Interface Science 678 (2025) 336-342.

[3] X. Han, X. Meng, S. Chen, J. Zhou, M. Wang, L. Sun, Y. Jia, X. Peng, H. Mai, G. Zhu, J. Li, C.W. Bielawski, J. Geng, P-Doping a Porous Carbon Host Promotes the Lithium Storage Performance of Red Phosphorus, ACS Applied Materials & Interfaces 15(9) (2023) 11713-11722.

[4] B. Xing, F. Shi, Z. Jin, H. Zeng, X. Qu, G. Huang, C. Zhang, Y. Xu, Z. Chen, J. Lu, A facile ice-templating-induced puzzle coupled with carbonization strategy for kilogram-level production of porous carbon nanosheets as high-capacity anode for lithium-ion batteries, Carbon Energy 6(12) (2024) e633.

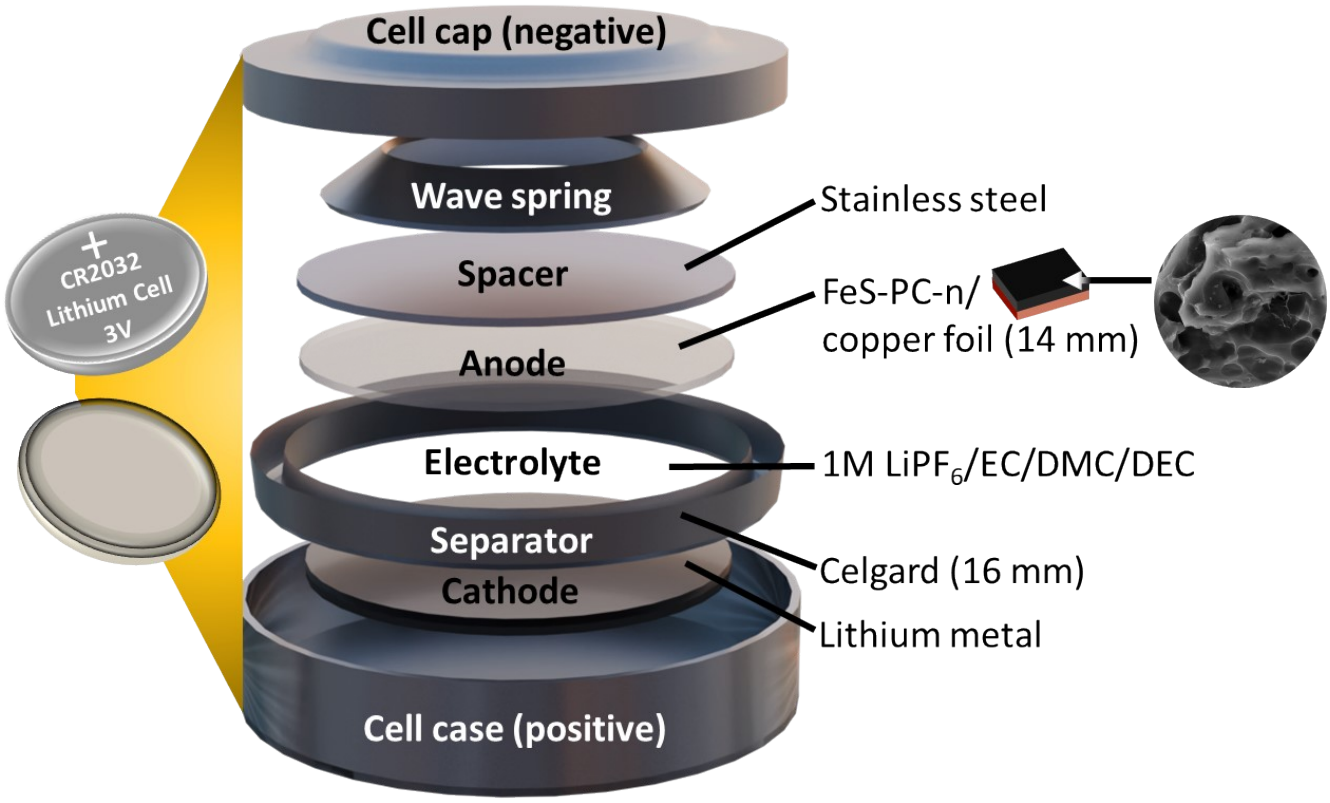

Scheme S1: Schematic representation of the coin cell lithium-ion battery assembly by using iron sulfide incorporated high surface area nanoporous carbon as an anode material.

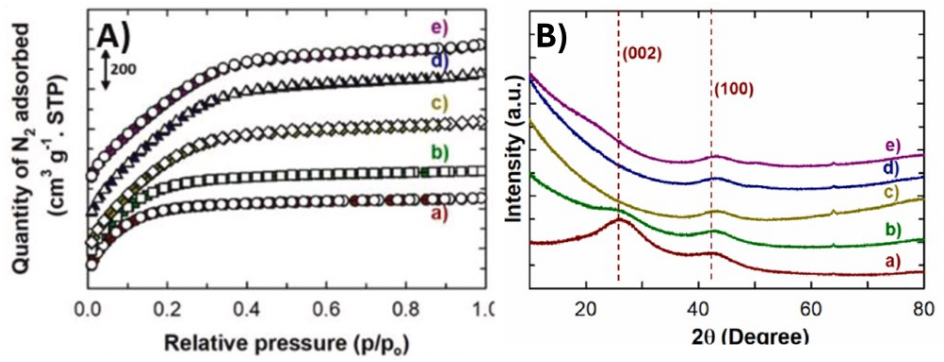

Figure S1: The N_2 sorption isotherm and XRD pattern of ASPC5-4 (labelled as d in both figures), which was published in our previous report [1].

[1] A.M. Ruban, G. Singh, R. Bahadur, C.I. Sathish, A. Vinu, Almond skin derived porous biocarbon nanoarchitectonics with tunable micro and mesoporosity for CO_2 adsorption and supercapacitors, Carbon 228 (2024) 119372.

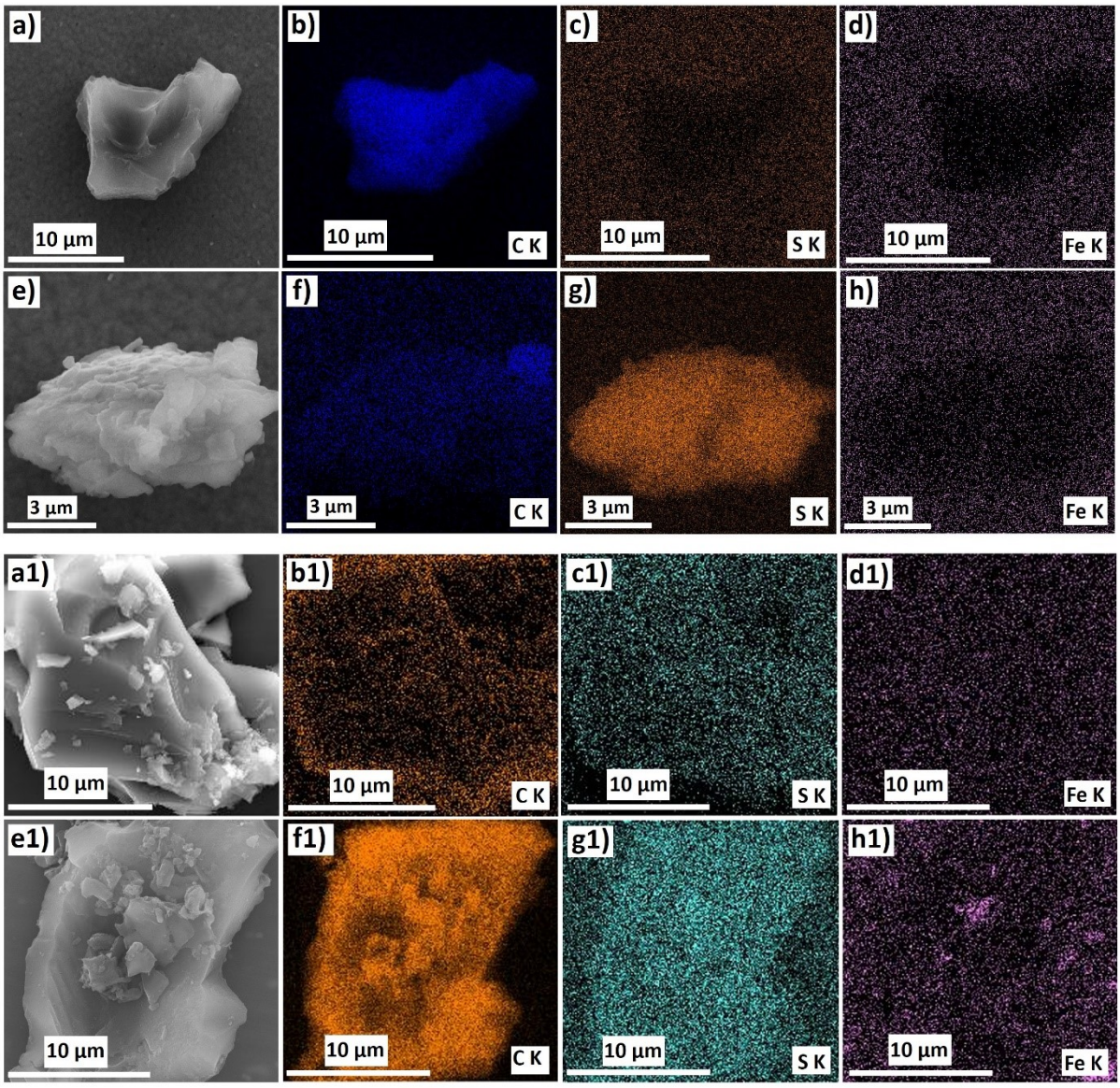

Figure S2: SEM images and elemental mapping of **a-d & a1-d1)** FeS-PC-1 and of **e-h & e1-h1)** FeS-PC-3 obtained at two different areas.

These EDS results highlight that the distribution of elements is uniform, however, the content of the elements varies from area to area.

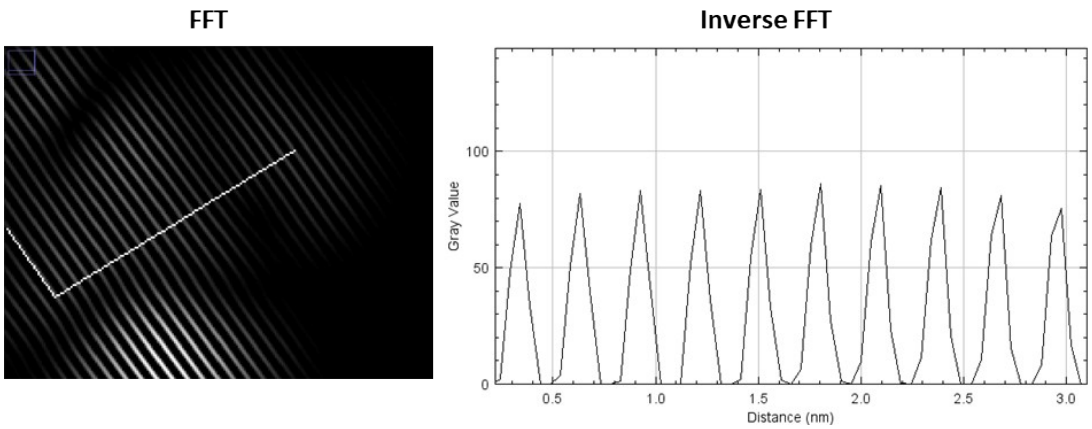

Figure S3: FFT and inverse FFT images used to calculate the lattice fringe in the TEM imgae provided in **Figure 1d**.

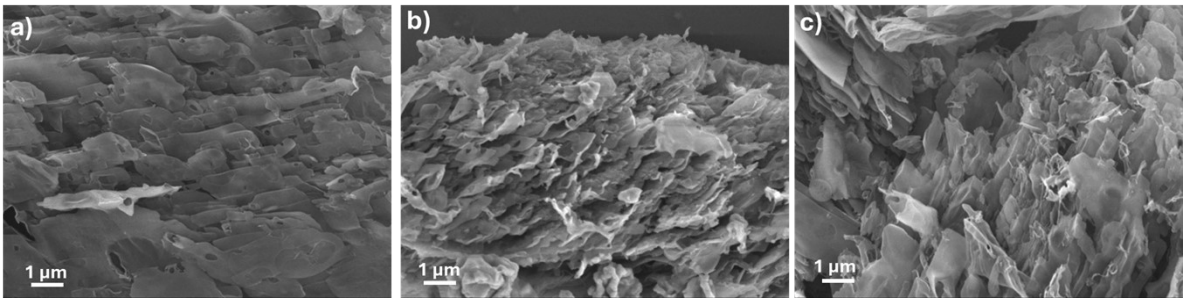

Figure S4: SEM images of **a)** 20Fe 100S **b)** 20Fe 150S and **c)** 20Fe 200S

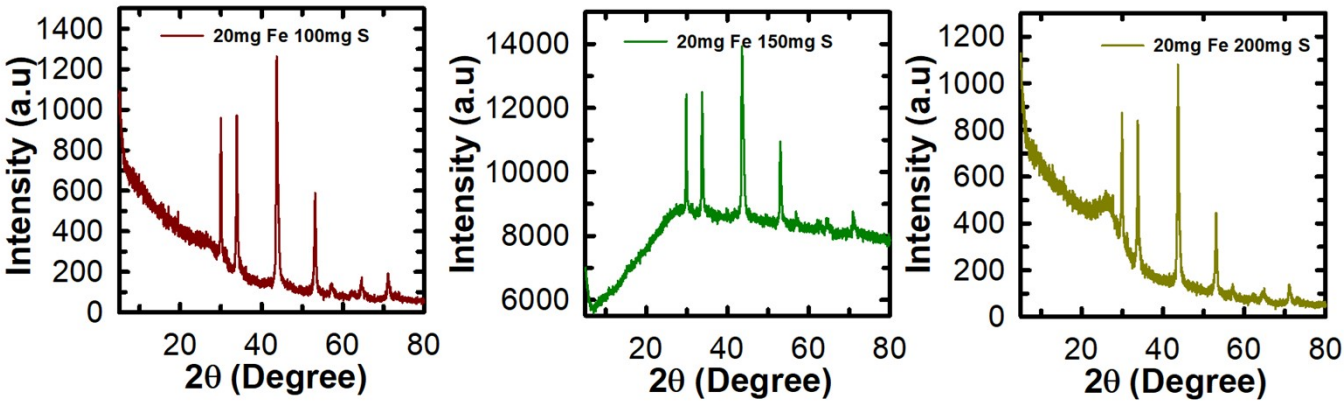

Figure S5: The x-ray diffraction pattern of FeS nanoparticles developed through direct carbonization of **a)** 20 mg iron acetate and 100 mg dithiooxamide, **b)** 20 mg iron acetate and 150 mg dithiooxamide, and **c)** 20 mg iron acetate and 200 mg dithiooxamide at 600 °C.

These XRD patterns confirm the formation of the FeS nanoparticles through direct carbonization of iron acetate (20 mg) and dithiooxamide (150 mg) at 600 °C. The intensity of the peaks is much higher than compared of the materials synthesized with porous carbon, as shown in **Figure 1a**. The presence of porous carbon as a support material provides stability to the structure and allows for higher mass transport during the process of lithiation and delithiation.

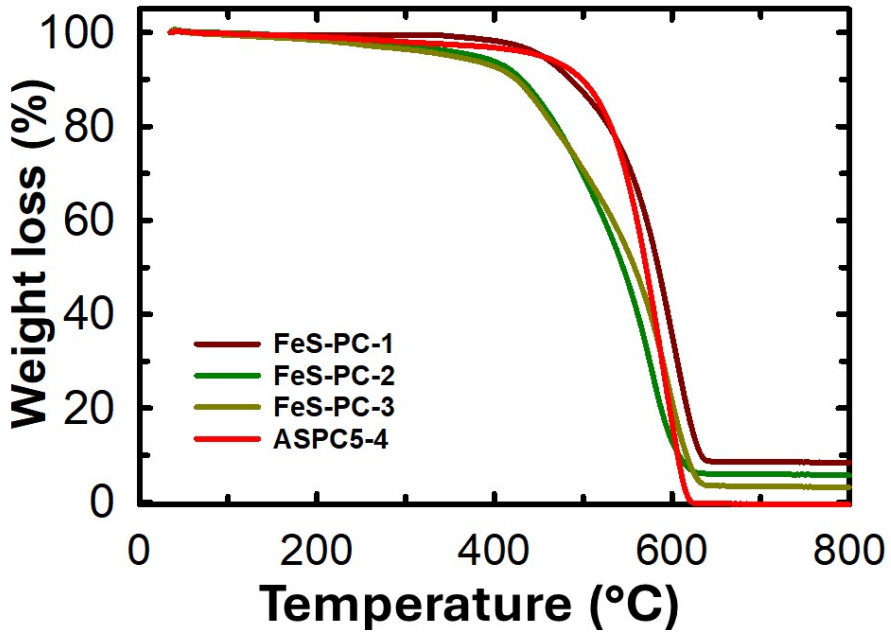

Figure S6: TGA analysis of porous carbon ASPC5-4, FeS-PC-1, FeS-PC-2, and FeS-PC-3

From the TGA, it is observed that there is an increased weight loss from FeS-PC-1 to FeS-PC-3. This may arise due to the increase in the amount of S in the composition. In the air atmosphere, sulfur oxidizes into gaseous SO_2/SO_3, which leads to further weight loss in addition to carbon combustion. The decreased residual mass seen in FeS-PC-3 supports this hypothesis by demonstrating that there is a higher volatile sulfur content corresponding to the increase in DTO, which acts as the S source.

The quantification of FeS in the synthesized materials was done as per the following.

1. For pure carbon ASPC5-4, the whole of the carbon was lost via oxidation and degradation in the air atmosphere.

2. The oxidation of FeS proceeds as per the following reaction at temperatures >500 °C.

$4FeS + 7O_2 \rightarrow 2Fe_2O_3 + 4SO_2$

So therefore, 4 mol FeS = 2 mol Fe_2O_3 which is 351.64 g FeS to 319.38 g Fe_2O_3

The mass ratio of Fe2O3 to FeS is 319.38/351.64 = 0.908

So 1g FeS produces 0.908 g of Fe_2O_3

Estimated FeS in the materials (a) = x mg of residue left/0.908

Estimated FeS content in % = (a)/initial mass*100

For **FeS-PC-1**

Initial mass – 5.8106

Weight loss - 91.65 %

Weight left – 0.4852

FeS content = 0.4852/0.908 = 0.53 mg

%FeS = 0.53/5.8106*100 = 9.1%

For **FeS-PC-2**

Initial mass – 3.295351

Weight loss – 94.56 %

Weight left – 0.179261

FeS content = 0.179261/0.908 = 0.20

%FeS = 0.20/3.295351*100 = 5.99%

For **FeS-PC-3**

Initial mass – 4.398985

Weight loss – 97.0738%

Weight left – 0.128725

FeS content = 0.128725/0.908 = 0.14

%FeS = 0.14/4.398985*100 = 3.22%

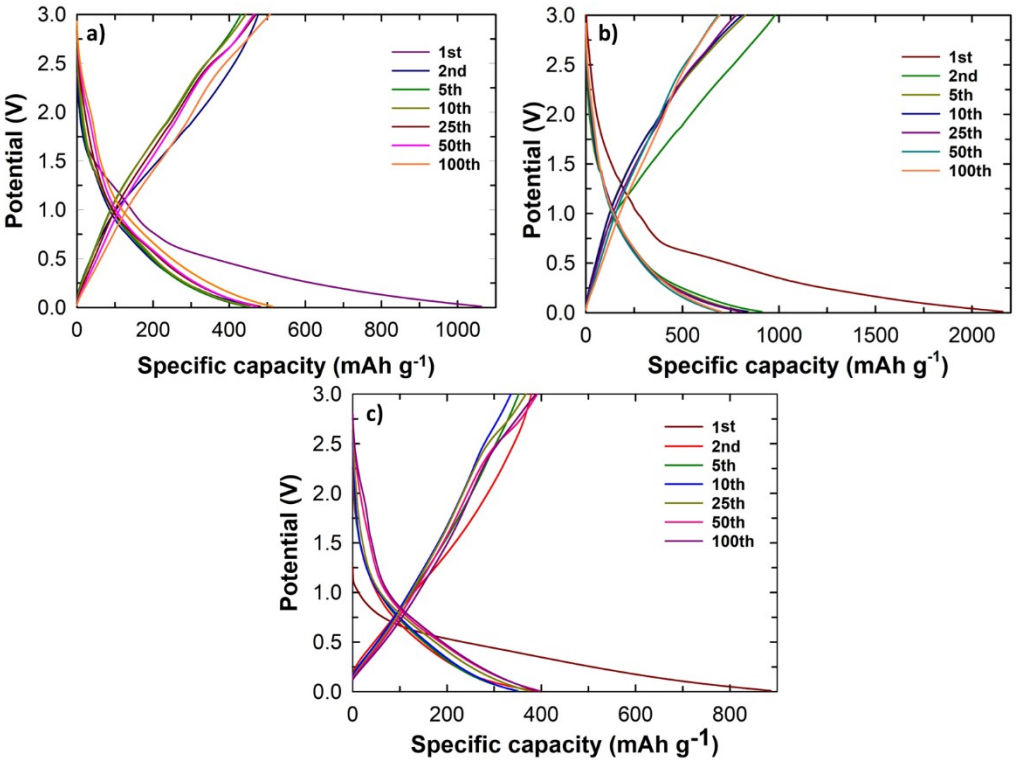

Figure S7: Charge-discharge profiles of **a)** FeS-PC-1, **c)** FeS-PC-3 and **c)** ASPC-5-4

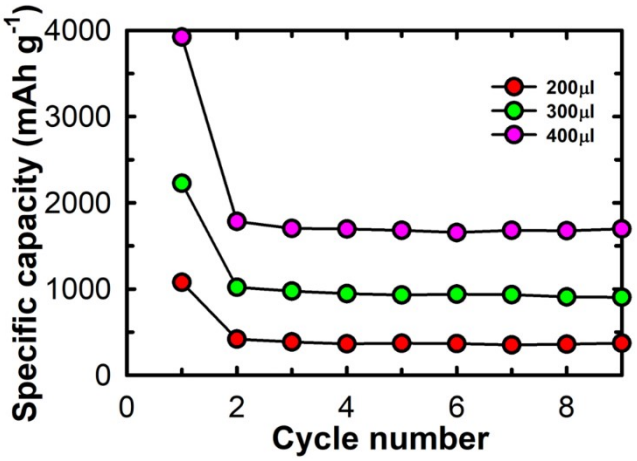

Figure S8: Rate capability test runs for FeS-PC-2 using different amounts of electrolyte

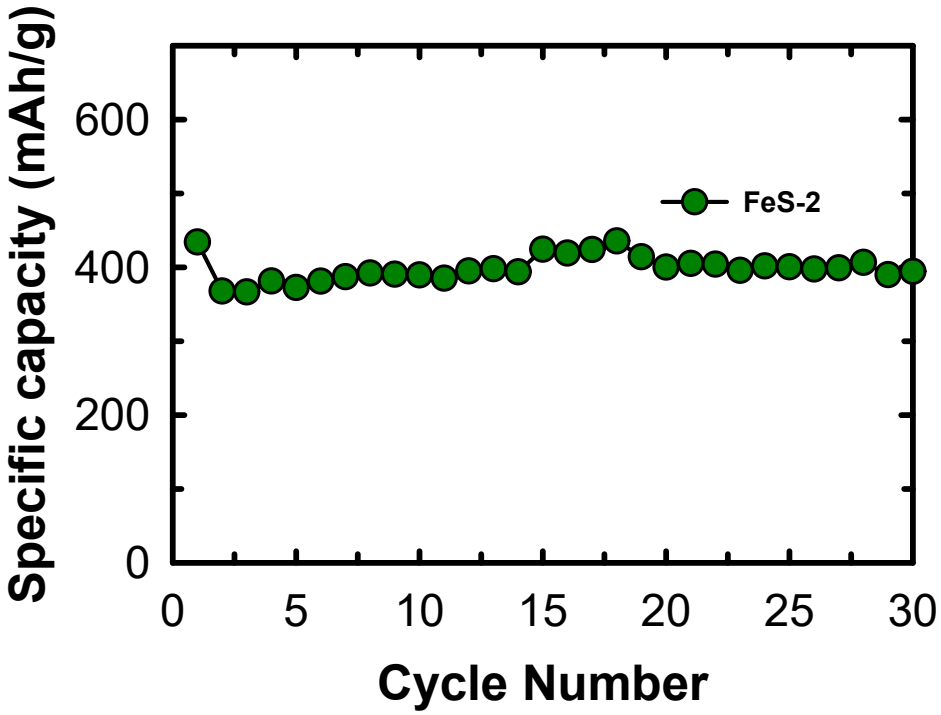

Figure S9: Lithium ion cycling performance of material synthesized using direct carbonization of 20 mg iron acetate and 150 mg of DTO

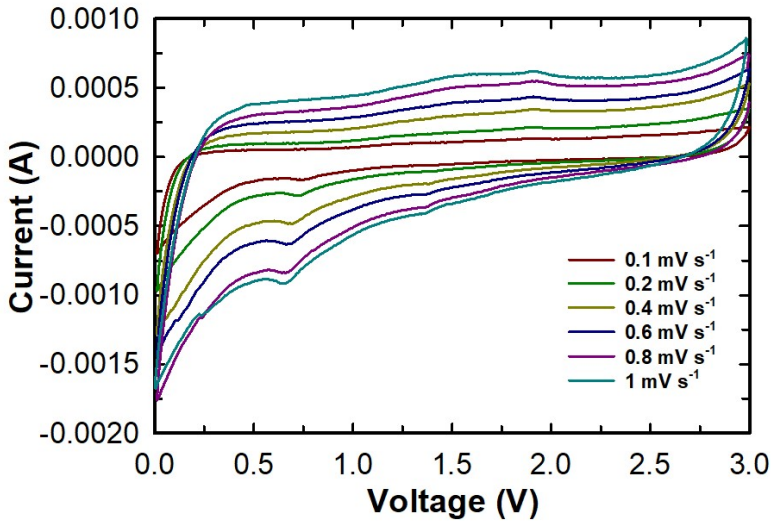

Figure S10: Cyclic voltametric plots of FeS-PC-2

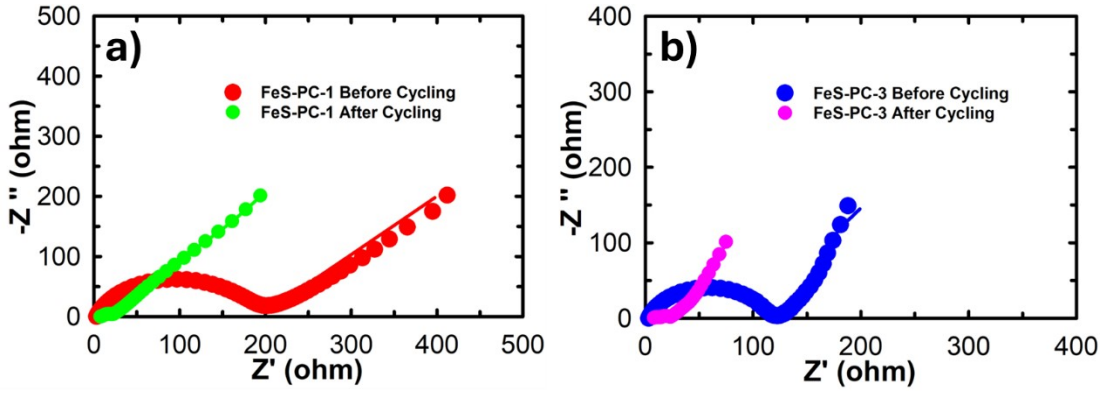

Figure S11: Nyquist plots of **a)** FeS-PC-1, and **b)** FeS-PC-3 before and after cycling

These results highlight that the R_{CT} value before cycling is higher in both materials (large semicircle) as compared to after cycling (small semicircle width).

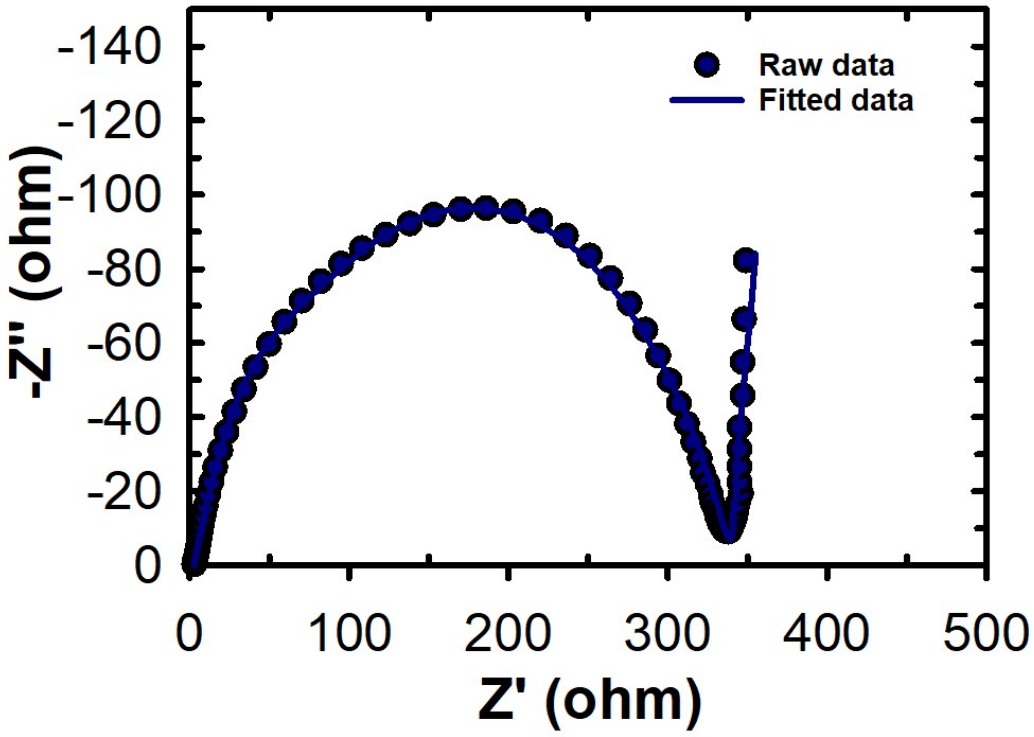

Figure S12: Nyquist plot of ASPC5-4

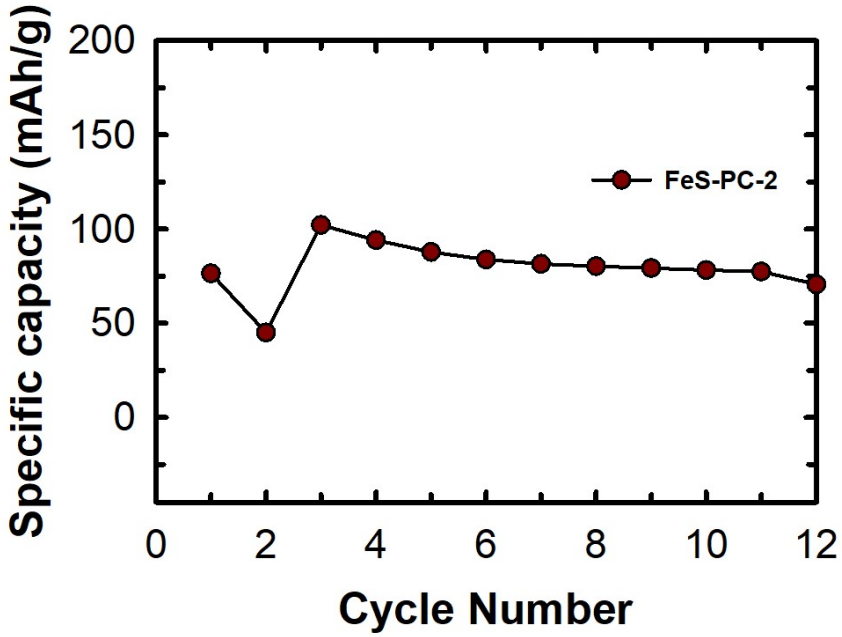

Figure S13: Cycling performance of the full cell

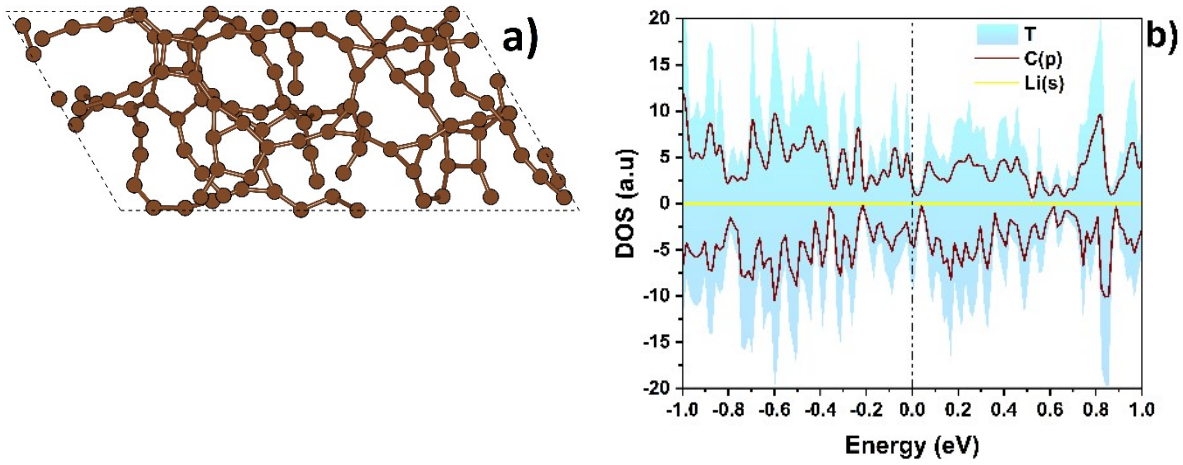

Figure S14: a) Top view of the optimized structure of PC bulk structure, **b)** total(T) DOS along with C(p) and Li(s) state contributing plot for the PC bulk structure. Dotted vertical line presents the Fermi level. (color; Brown: Carbon).

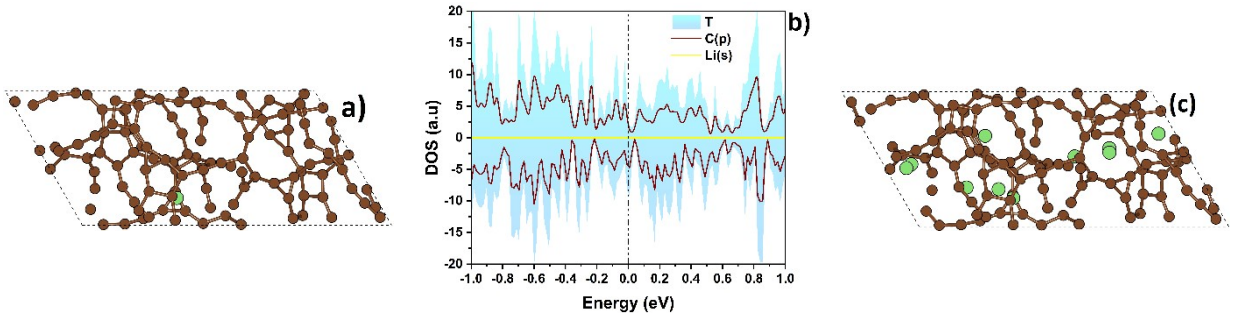

Figure S15: a) Top view of the optimized structure of the PC-mLi (where m = 1), **b)** spin-polarized partial density of states of PC-1Li. The black dotted line presents the Fermi Level, **c)** Top view of the optimized structure of the PC-mLi (where m = 10). (color; Brown: Carbon, Lime Green: Lithium).

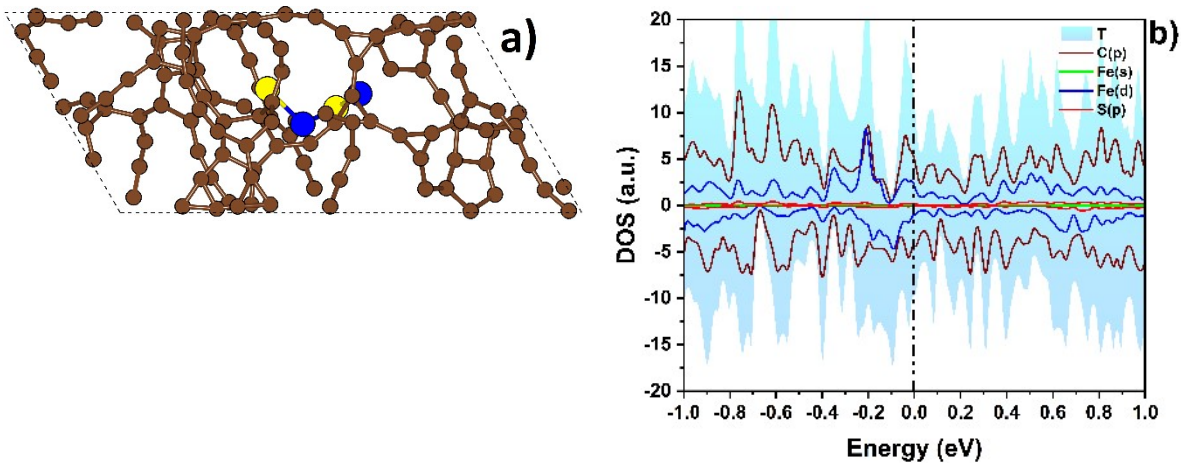

Figure S16: a) Top view of the optimized structure of PC-Fe_2S_2, **b)** total(T) DOS along with C(p) and Li(s) state contributing plot for the PC-Fe_2S_2 structure. Dotted vertical line presents the Fermi level. (color; Blue: Ferrous, Brown: Carbon, Chartreuse Yellow: Sulphur, Lime Green: Lithium).

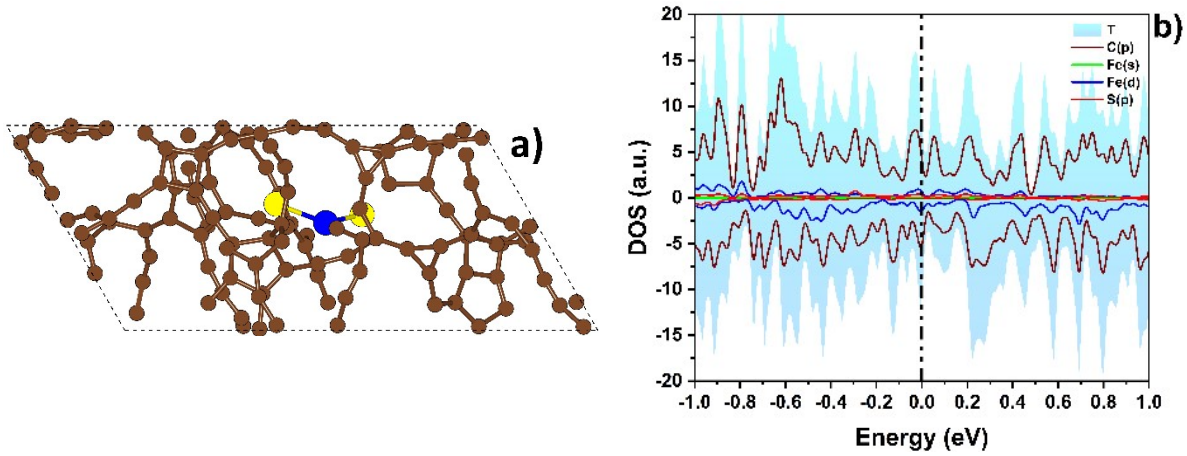

Figure S17: a) Top view of the optimized structure of PC-FeS_2, **b)** total(T) DOS along with C(p) and Li(s) state contributing plot for the PC-FeS_2 structure. Dotted vertical line presents the Fermi level. (color; Blue: Ferrous, Brown: Carbon, Chartreuse Yellow: Sulphur, Lime Green: Lithium).

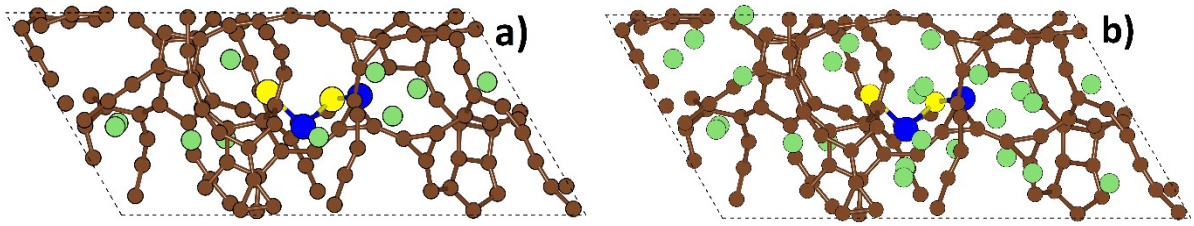

Figure S18: a) Top view of the optimized structure of PC-Fe_2S_2-10Li and PC-Fe_2S_2-25Li (color; Blue: Ferrous, Brown: Carbon, Chartreuse Yellow: Sulphur, Lime Green: Lithium).

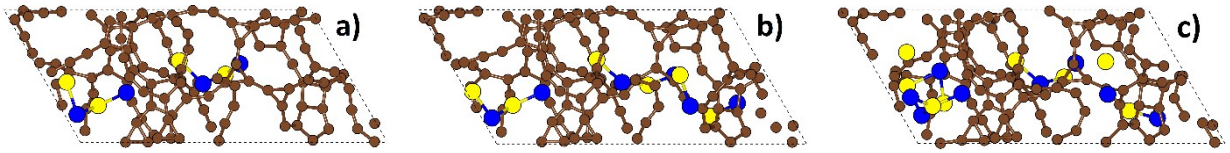

Figure S19: a-c) Top view of the optimized structure of PC-nFe_2S_2, where n=2,3,4.